Journal of Materials Chemistry A

Accepted Manuscript

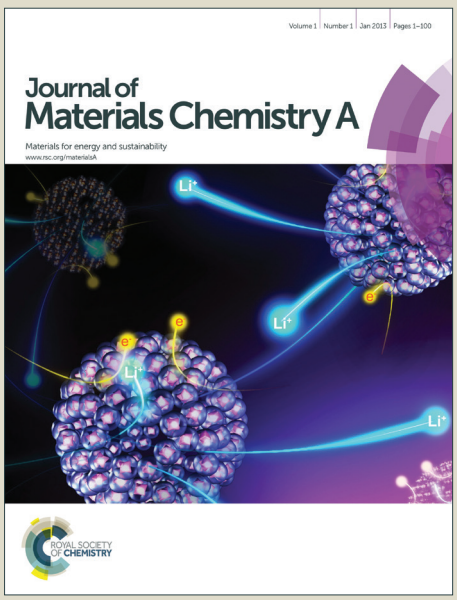

ROYAL SOCIETY OF CHEMISTRY

www.rsc.org/materialsA

Journal Name

RSCPublishing

COMMUNICATION

Active $LaNi_{1-x}Fe_xO_3$ Bifunctional Catalysts for Air Cathodes in Alkaline Media

Cite this: DOI: 10.1039/x0xx00000x

Daiwei Zhang,[a,b,c] Yufeng Song,[a] Zhenzhen Du,[a] Long Wang,[b] Yutao Li,[b] John B. Goodenough*[b]

Received ooth January 2012,
Accepted ooth January 2012

DOI: 10.1039/x0xx00000x

www.rsc.org/

$LaNi_{1-x}Fe_xO_3$ (x = 0, 0.1, 0.2, 0.6) were synthesized by the sol-gel method. The Fe-substitution for Ni suppresses the formation of Ni^{II} on the perovskite surface and creates a stronger surface Ni-O bond. This study exhibits the possibility to adjust the bi-functional activity of $LaNiO_3$ through a simple doping process.

Electrochemical cells with an air cathode are of great interest, but the cost, activity, and life of the air-cathode catalysts for the oxygen-reduction and oxygen-evolution reactions (ORR and OER) have prevented commercial viability of room-temperature metal/air batteries and hydrogen/air fuel cells.[1-7] The cost and instability of noble-metal catalysts[8,9] has shifted attention to oxide catalysts.[10,11] Platinum-gold nanoparticles have shown good activity for both the ORR and OER,[12] but the limited availability and high cost of noble-metal bi-functional catalysts prevent their large-scale applications. Therefore it is important to seek cost-effective, corrosion-resistant, and highly active bi-functional oxide catalyst for both the ORR and OER kinetics for air cathodes of electrochemical cells.

Perovskite materials have been widely used as catalysts for fuel cells and metal-air batteries owing to their mixed oxide-ion/electronic conductivity and low cost. R. Chiba *et al.*[13] have shown that $LaNi_{0.6}Fe_{0.4}O_3$ is a viable cathode catalyst for the ORR at the cathode of a solid oxide fuel cell with an electronic conductivity of 580 S/cm at 800°C and a relatively low thermal expansion coefficient. However, $LaNi_{1-x}Fe_xO_3$ materials prepared in this article just showed good performance in a lower temperature range. Suntivich *et al.*[14,15] have reported oxides with the perovskite structure that contain a single σ-bonding electron (e^1 configuration) at the surface cations can show comparable ORR and OER activities to those reported for platinum-based metal catalysts in alkaline solution. These authors also pointed out that a strong admixture of O-*2p* character into the active *d*-electron redox couple is also important for the OER. W. Zhou *et al.*[16] have pointed out that the cubic $LaNiO_3$ phase shows higher ORR and OER activity relative to the rhombohedral phase. Jaka Sunarso *et al.*[17] have pointed out that the presence of certain transition-metal elements in the B-site cation can have a significant impact on both ORR rates (e.g., with Mn, Co and Ni) and high chemical and electrochemical stability (e.g., Cr and Fe) in alkaline solution. Using Ni foam as substrate, Costa *et al.*[18] have shown that perovskite $LaNi_{0.93}Cu_{0.05}O_3$ powders give an excellent OER in alkali solution. In addition, several other oxides with the perovskite structure have been reported to be bifunctional catalysts for the ORR and OER, *e.g.* honeycomb-like $LaNi_{0.85}Mg_{0.15}O_3$,[19] urchin-like $La_{0.8}Sr_{0.2}MnO_3$,[20] nanoporous $La_{0.6}Ca_{0.4}CoO_3$,[21] and hierarchal $La_{0.5}Sr_{0.5}CoO_{2.91}$.[22]

The perovskite $LaNiO_3$ is metallic as a result of strong O-*2p* covalent admixture into the partially filled, σ-bonding e orbitals of low-spin Ni^{III}: t^6e^1.[23] Therefore, $LaNiO_3$-based perovskites offer promise of providing bifunctional ORR and OER catalytic activity provided the surface nickel retain the Ni^{III} valence state. Lanthanum ferrite ($LaFeO_3$) is expected to be more stable than nickel perovskites because the Fe^{3+} has a stable electronic configuration $3d_5$.[24] And the Fe-based catalyst also demonstrated a high activity for the decomposition of the HO_2^- intermediate.[25] In this paper, we report bifunctional ORR and OER activity of $LaNi_{1-x}Fe_xO_3$ and show that the Fe stabilizes low-spin surface Ni^{III} versus Ni^{II}: t^6e^2.

A series of $LaNi_{1-x}Fe_xO_3$ perovskite nanoparticles were prepared by the sol-gel method as described in detail elsewhere.[26] Briefly, $La(NO_3)_3 \cdot xH_2O$ and transition-metal nitrates (Sinopharm, reagent grade) were dissolved in deionized water. Subsequently, the above metal nitrates solution was gradually added to a mixed solution of citric acid ($HOC(COOH)(CH_2COOH)_2$, ≥ 99.5%) and ethylene glycol ($HOCH_2CH_2OH$, 99.8%) under vigorous stirring conditions at 60°C. The mixture was then heated to 80°C to form a viscous gel, which was heated at 250°C until an amorphous citrate precursor was obtained. The precursor was milled and finally sintered at 750°C under air

atmosphere for 2 h to remove residual carbon and form perovskite oxide powders with well-crystallized structure.

The crystal phase and purity of the as-prepared powders were determined by X-ray powder diffraction with a Cu Kα radiation of 1.54056 Å from 20° to 80°. Field-emission scanning electron microscope images were collected with a Hitachi SU8020 at an acceleration voltage of 3 kV. X-ray photoelectron spectra (XPS) were obtained on a Rigaku D/MAX2500V X-ray photoelectron spectrometer with an exciting source of Al Kα (1486.6 eV).

Heavy ORR or OER particles require an immobilizing binder to a metallic substrate that facilitates transport of dissolved O_2 in addition to electrons to or from the catalyst surface. Therefore, the oxide coating was dispersed as an ink on a glassy carbon (GC) electrode for thin-film rotating-disk-electrode (RDE) measurements. To form a homogeneous ink, 1 mg of the perovskite powder was mixed with 4.25 mg of XC-72 carbon and 64 µL of 5 wt% NAFION dispersed in 1 mL of 3:1 vol:vol water/isopropanol solution with about 40 min sonication. The glassy carbon disk electrodes (3 mm diameter, 0.071 cm^2 area) were polished with a 0.05 µm alumina slurry on a clean polishing cloth, rinsed with distilled water and ethanol, and then dried with N_2 before each experiment. An aliquot of 3 µL of suspension was drop-cast onto the processed glassy carbon, yielding a final composition with 0.2 mg- cm^{-2} of catalyst on the disk. The electrode was then dried slowly inside a closed container to obtain a film of catalyst particles deposited onto the glassy carbon electrode. In order to check the reproducibility of the film quality and performance, three glassy carbon electrodes coated with perovskite film were prepared for each sample. Rotating-disk electrode (RDE) measurements were employed to assess the ORR and OER kinetics of as-prepared catalysts. All electrochemical measurements were conducted in a three-electrode cell in O_2-saturated KOH electrolyte at room temperature with a sweep rate of 10 mV s^{-1}. The three-electrode configuration used for RDE measurements consisted of a platinum electrode as an auxiliary electrode, a saturated calomel electrode as a reference electrode, and the glassy carbon electrode as the working electrode. Prior to examining the ORR and OER performance, the glassy carbon electrode loaded with catalyst was immersed into the N_2-purged electrolyte for at least 30 min. After steady-state CVs were obtained in N_2, the gas line to supply O_2 was purged for another 30 min before the ORR polarization curve was tested from 0 V to -1.0 V vs. SCE; the ORR test was followed by a voltage scan from -0.2 to 1.2 V to examine the OER polarization curve. Electrochemical data that varied within the experimental error were collected with an Autolab electrochemical workstation. The electrochemical properties were carried out by assembling Li-O_2 batteries in a glove box filled with pure argon gas as described elsewhere[27,28]. Electrochemical tests were performed in a simple two-electrode cell with metallic lithium as the anode, tetra-ethylene glycol dimethyl ether (TEGDME) based electrolyte as the electrolyte, glass paper and two layers of Celgard® polypropylene as separator, and carbon-paper-supported catalysts as cathode electrodes. Galvanostatic charge-discharge cycling of the cells was studied in a potential range of 2.5-4.2 V vs. Li/Li^+ with a multichannel battery testing system (LAND CT 2001A).

The powder XRD patterns of the as-synthesized perovskite oxides presented in Figure 1 show that Fe-doped $LaNi_{1-x}Fe_xO_3$ (x =0, 0.1, 0.2) perovskites have the rhombohedral structure of $LaNiO_3$, space group $R\bar{3}c$ (PDF card no. 01-079-2451: a =5.457 Å, b = 5.457 Å, c = 13.160 Å), while $LaNi_{0.4}Fe_{0.6}O_3$ has the cubic structure of $LaNiO_3$, space group: Pm-3m (211) (JCPDS: 33-0710). Detailed analysis for $LaNi_{1-x}Fe_xO_3$ (x = 0, 0.1, 0.2) by a peak-matching procedure to the powder XRD database (PDF 22004) demonstrated a partial substitution of Ni by Fe does not produce any NiO second phase; however, NiO was detached in the x = 0.6 sample.

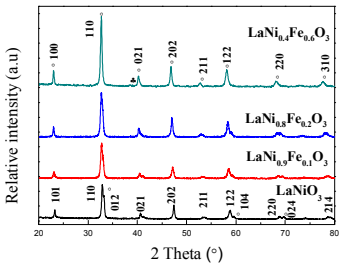

Figure 1. XRD patterns of $LaNi_{1-x}Fe_xO_3$ (x = 0, 0.1, 0.2, 0.6) perovskite oxides: (°) $LaNiO_3$; (♣) NiO.

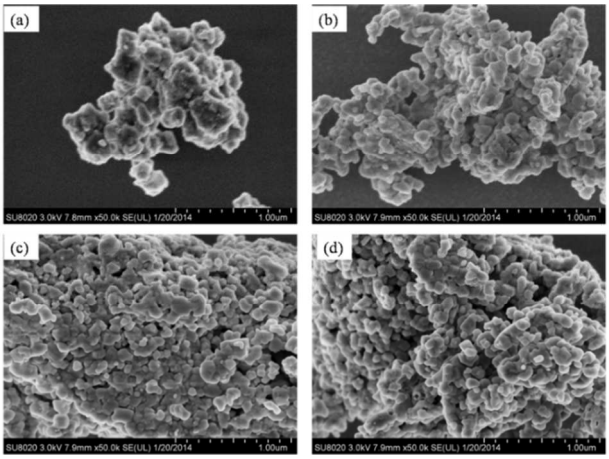

Figure 2. FESEM images of $LaNi_{1-x}Fe_xO_3$ (x = 0, 0.1, 0.2, 0.6) perovskite oxides.

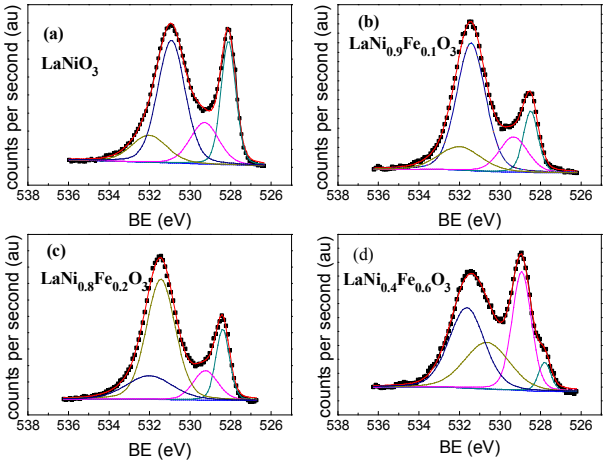

Figure 3. O: 1s spectra of $LaNi_{1-x}Fe_xO_3$ (x = 0, 0.1, 0.2, 0.6) perovskite oxides.

Catalyst	La $3d_{5/2}$	Ni $2p_{3/2}$	Fe $2p_{3/2}$	O 1s
$LaNiO_3$	834.7	854.5	—	528.6
		856.0		529.29
				531.01
				532.02
$LaNi_{0.9}Fe_{0.1}O_3$	834.6	854.3	710.7	528.07
		856.0		529.25
				531.0
				532.0
$LaNi_{0.8}Fe_{0.2}O_3$	834.7	854.3	710.6	528.4
		856.1		529.28
				531.06
				531.95
$LaNi_{0.4}Fe_{0.6}O_3$	834.6	854.4	710.7	527.98
		856.2		528.93
				530.94
				531.87

Table 1. Binding energies in eV obtained by XPS of $LaNi_{1-x}Fe_xO_3$ (x = 0, 0.1, 0.2, 0.6) catalysts.

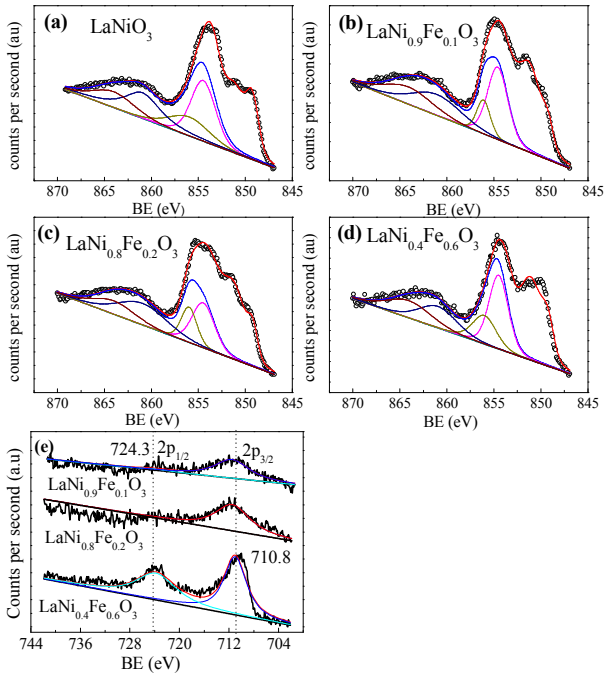

Figure 4(a)-(d) Ni: $2p_{3/2}$ spectra of $LaNi_{1-x}Fe_xO_3$ (x = 0, 0.1, 0.2, 0.6) perovskite oxides; (e) Fe: $2p_{3/2}$ spectra of $LaNi_{1-x}Fe_xO_3$ (x = 0.1, 0.2, 0.6) perovskite oxides.

Fig.2 shows that the morphologies of the as-synthesized perovskite powders were agglomerates in the whole range of $LaNi_{1-x}Fe_xO_3$ (x = 0, 0.1, 0.2 and 0.6). The primary particle size decreased gradually from ~200 nm of $LaNiO_3$ (Fig. 2a) to ~100 nm of $LaNi_{0.4}Fe_{0.6}O_3$ (Fig. 2d).

The relative abundance of surface chemical species was probed by X-ray photoelectron spectroscopy (XPS). The binding energies of La: $3d_{5/2}$, Ni: $2p_{3/2}$, Fe: $2p_{3/2}$ and O: 1s presented in Table 1 are in accordance with values reported previously.[29-31] The O: 1s XP-spectra of the $LaNi_{1-x}Fe_xO_3$ (x = 0, 0.1, 0.2, 0.6) perovskites measured at normal emission angles are presented in Figure 3. The O: 1s peaks are complex and consistent with the existence of more than one type of oxygen species in the surface layer. Upon deconvolution, the components at the low binding energies (528.6 eV and 529.3 eV) are assigned to lanthanum and nickel bonded to lattice oxide ions; the components at the high binding energies (531.01 eV and 532.02 eV) are assigned to nickel and lanthanum with a hydroxyl ($-OH^-$) ligand.[25] As presented in Figure 3, the latter two peaks at higher energy become stronger with larger Fe doping, indicating an increase of adsorbed hydroxyl on the surface of the catalyst. It has been suggested that the ORR kinetics is limited by the rate of O_2^{2-}/OH^- displacement and OH^- regeneration.[15] It has also been pointed out that the concentration of the hydroxyl oxygen ($-OH^-$) on the surface of perovskite oxide catalysts governs the OER rate.[14,30,32]

Figure 4(a)-(d) displays the Ni: $2p_{3/2}$ XP-spectra of $LaNi_{1-x}Fe_xO_3$ (x = 0, 0.1, 0.2, 0.6) perovskites. The La: $3d_{3/2}$ and Ni: $2p_{3/2}$ XP-spectra in the high binding energies are partially overlapping; we first fitted the La: $3d_{3/2}$ XP-spectra and then subtracted it to analyze accurately the Ni valence and its content on the catalyst surface. Upon deconvolution, two Ni: $2p_{3/2}$ peaks corresponding to Ni^{II} (about 854 eV) and Ni^{III} (about 856 eV) can be observed. The signal fraction of the Ni species with lower oxidation state (Ni^{II}) diminishes with the replacement of Ni by Fe in the range of $0 \le x \le 0.2$, indicating that small amounts of Fe additives stabilize surface Ni^{III}.

The Fe $2p_{3/2}$ region (Fig. 4(e)) shows a band wide enough to include contributions from Fe-O-M (710.8 eV) oxidation states, indicating the existence of Fe^{3+} ions in the $LaNiO_3$ perovskite structure.

Table 2 summarizes the surface compositions obtained by XPS and bulk compositions obtained by EDS (Figure 5). We observed that the Ni/La and Fe/La ratios of the bulk are close to the theoretical molar ratio while the material surface shows a relatively Ni-rich composition. A jump of Ni ratio on the material surface was observed at the highest Fe-doping condition $LaNi_{0.4}Fe_{0.6}O_3$, which was due to the leaching out of NiO from the surface as indicated by XRD in Fig. 1. This result suggests that Fe-doping ($0 \le x \le 0.2$) successfully suppressed the formation of NiO on the surface of $LaNiO_3$[19], which has been previously deduced from the XRD patterns. Since NiO is inactive for both the ORR and OER, the existence of NiO on the surface blocks the active sites as shown in the electrochemical measurements below. The resulting increase Ni^{III} on the surface is beneficial for both the ORR and OER which is in accordance with the hypothesis of Suntivich *et al.*[14,15].

The activities of the $LaNi_{1-x}Fe_xO_3$ catalysts for the ORR and OER in O_2-saturated 0.1 M KOH was evaluated with rotating-disk-electrode (RDE) measurements. Figure 6 (a)-(e) shows typical ORR current densities under different rotation rates from 0 to 2000 rpm. At a potential more negative than approximately 0.51 V vs. SCE, the current plateau indicates the diffusion-limited region. The electrochemical process gradually changes from a transient behavior to a steady-state curve on increasing the rotation rate from 0 to 2000 rpm.

For a more quantitative analysis of the ORR catalyzed by $LaNi_{1-x}Fe_xO_3$, the current-potential curves of Figure 6 (a)-(e) were also analyzed with the Koutecky-Levich equation:

$$i^{-1} = -(nkFAC_{O2})^{-1} - (0.62nFAD_{O2}^{2/3}\nu)^{-1} - (6C_{O2}\omega^{1/2})^{-1}$$

where n is the number of transferred electrons in the overall reduction process, k is the Boltzmann constant. F is the Faraday constant, C_{O2} is the saturated concentration of oxygen in 0.1 M KOH solution, A is the geometric area of the disk electrode, ω is the electrode rotation rate,

D_{O_2} is the diffusion coefficient of oxygen, and υ is the kinematic viscosity of the solution. Figure 6 (f) shows the Koutecky-Levich plots for the experimental data taken at -0.6 V. All plots demonstrate linear

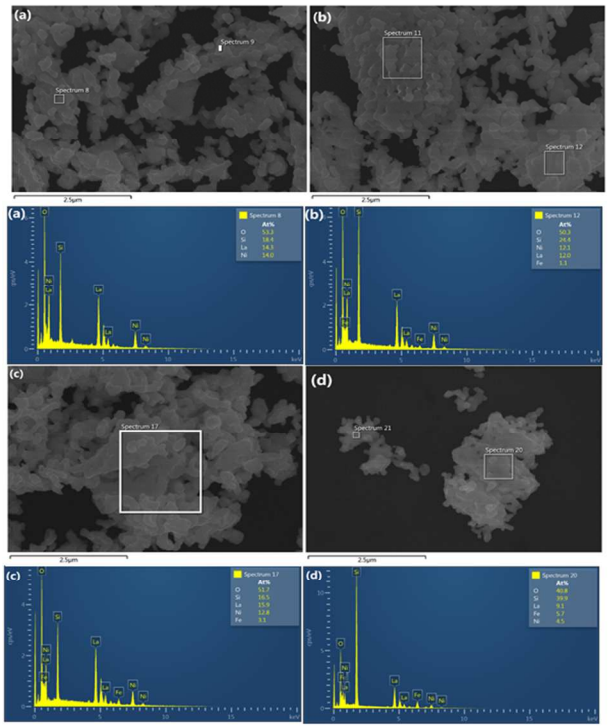

Figure 5. EDS of $LaNi_{1-x}Fe_xO_3$ (x = 0, 0.1, 0.2, 0.6) perovskite oxides.

Catalyst	Surface(XPS)			Bulk (EDS)		
	Ni/La	Fe/La	O/La	Ni/La	Fe/La	O/La
$LaNiO_3$	1.51	----	5.50	0.979	----	3.727
$LaNi_{0.9}Fe_{0.1}O_3$	1.24	0.07	4.77	1.008	0.092	4.192
$LaNi_{0.8}Fe_{0.2}O_3$	1.06	0.20	4.07	0.805	0.195	3.208
$LaNi_{0.4}Fe_{0.6}O_3$	1.48	0.31	4.26	0.495	0.626	4.484

Table 2. Composition (atomic %) obtained by XPS (not including carbon) and EDS (not including Si) of $LaNi_{1-x}Fe_xO_3$ (x = 0, 0.1, 0.2, 0.6) catalysts.

features, implying a first-order dependence of the O_2 reaction kinetics on all the perovskite oxides. The overall ORR electron transfer numbers are, respectively, 2.1, 2.3, 3.7, 3.9, and 3.8 for XC - 72 and x = 0, 01, 0.2, 0.6. The overall electron transfer number of $LaNi_{0.9}Fe_{0.1}O_3$, $LaNi_{0.8}Fe_{0.2}O_3$, and $LaNi_{0.4}Fe_{0.6}O_3$ nanoparticles is n = 3.9, quite close to the theoretical value (4.0) for the ORR in alkaline solution; the right amount of Fe doping can alter the ORR mechanism from a 2-electron dominated pathway (reduction of O_2 to HO_2^-) to a 4-electron dominated reduction of O_2 to OH^- in alkaline electrolyte.

Figure 7 (a) shows the linear scanning voltammograms representing the ORR in O_2-satured 0.1 M KOH electrolyte on a thin film of the $LaNi_{1-x}Fe_xO_3$ oxides on the rotating-disk working electrode. It can be seen that the rhombohedral $LaNi_{0.8}Fe_{0.2}O_3$ catalyst exhibits the most positive ORR onset potential and an ORR diffusion-limiting current density as high as that with cubic $LaNi_{0.4}Fe_{0.6}O_3$, which is inconsistent with the report of Wei Zhou *et al.*[16] Trace amounts of NiO can be detected on the surface of the cubic $LaNi_{0.4}Fe_{0.6}O_3$ phase, which degrades the electrochemical performance.

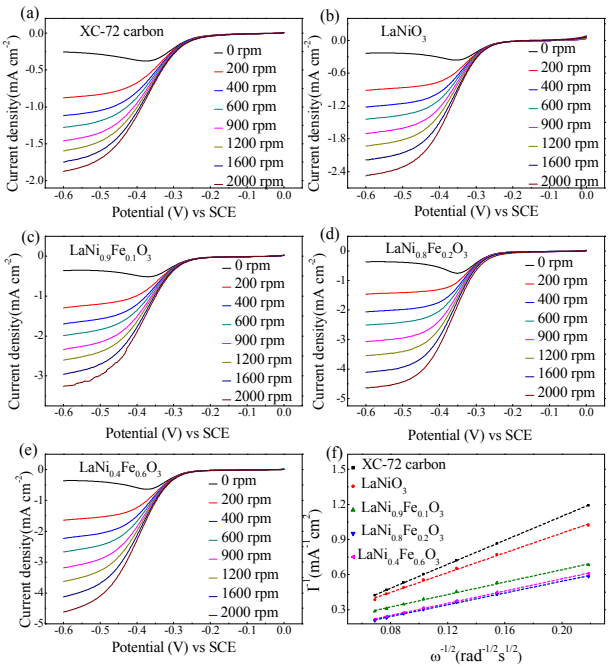

Figure 6. ORR polarization curves of (a) XC - 72, (b) $LaNiO_3$, (c) $LaNi_{0.9}Fe_{0.1}O_3$, (d) $LaNi_{0.8}Fe_{0.2}O_3$, (e) $LaNi_{0.4}Fe_{0.6}O_3$ in O_2-saturated 0.1 M KOH with a sweep rate of 10 $mV \cdot s^{-1}$ under different rotation rates; (f) Koutecky-Levich plots of $LaNi_{1-x}Fe_xO_3$ (x = 0, 0.1, 0.2, 0.6) based on ORR polarization curves at -0.6 V.

$LaNi_{1-x}Fe_xO_3$ (x = 0, 0.1, 0.2, 0.6) are bi-functional electrocatalysts, not only good for ORR, but even better for OER compared with Pt/C (20%) (Fig. S1). Figure 7 (b) shows the OER reactivity of as-prepared $LaNi_{1-x}Fe_xO_3$ catalysts coated onto glassy carbon electrodes with a rotation rate of 1600 rpm. The OER onset potential for $LaNiO_3$ is 0.64 V vs SCE and the OER diffusion-limiting current density is 6.7 mA cm^{-2}. The OER onset potential for the $LaNi_{0.8}Fe_{0.2}O_3$ and $LaNi_{0.4}Fe_{0.6}O_3$ are approximately 0.6 V while the ORR for the $LaNi_{0.4}Fe_{0.6}O_3$ catalyst is far more negative. The OER diffusion-limiting current density of $LaNi_{0.4}Fe_{0.6}O_3$ (56 mA cm^{-2}) is close to $LaNi_{0.8}Fe_{0.2}O_3$ (54 mA cm^{-2}) at 1.2 V. The better OER activity of Fe-doped $LaNiO_3$ can be ascribed to an increase with Fe doping in the electron transfer from surface oxygen to the lattice Ni with increasing surface-Ni valence, which promotes attack of the surface oxygen by electrolyte oxygen.

Figure 7 (c) displays the OER polarization curves of $LaNi_{0.8}Fe_{0.2}O_3$ at the 1st cycle, 100th cycle, 300th cycle, 500th cycle in an O_2 saturated aqueous electrolyte, 0.1 M KOH with a sweep rate of 10 mVs^{-1} between -0.2 V and 1.2 V at a rotating speed of 1600 rpm. The $LaNi_{0.8}Fe_{0.2}O_3$ clearly shows an outstanding catalytic durability within the 300 cycles. Only after 500 cycles does the material show a current decrease of 19% of the initial value at 1.2 V (vs. SCE). Potential causes of this attenuation have been suggested, such as changes in the electrode microstructure, aggregation of the electrocatalyst or changes of the electrolyte concentration[33].

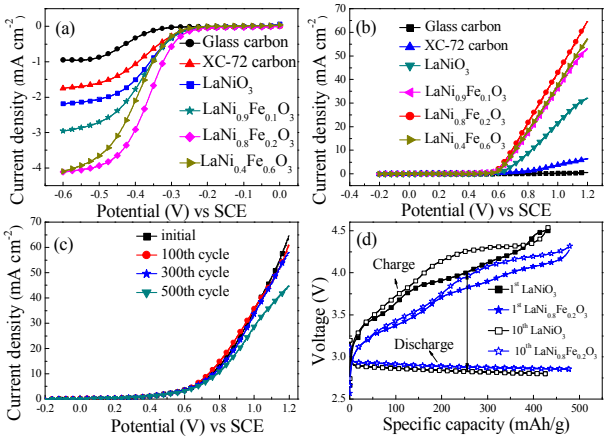

Figure 7 (a) ORR and (b) OER polarization curves of $LaNi_{1-x}Fe_xO_3$ (x = 0, 0.1, 0.2, 0.6); (c) OER polarization curves of $LaNi_{0.8}Fe_{0.2}O_3$ at the 1st cycle, 100th cycle, 300th cycle, 500th cycle in O_2 saturated aqueous electrolyte, 0.1 M KOH with a sweep rate of 10 mVs^{-1} at 1600 rpm; (d) Charge/Discharge curves of Li-air batteries with $LaNiO_3$ and $LaNi_{0.8}Fe_{0.2}O_3$ perovskite oxides as the air electrode

Figure 7 (d) shows the electrocatalytic performance of $LaNiO_3$ and $LaNi_{0.8}Fe_{0.2}O_3$ as the cathode catalysts for Li-O_2 batteries with 1 M $LiPF_6$/ Tetraethylene glycol dimethyl ether (TEGDME) electrolyte within a potential range of 2.5-4.5 V. The discharge/charge depths were controlled between 400~500 mA h/g. The round trip efficiencies (ORR/OER) at first cycle were 76% and 72% for $LaNi_{0.8}Fe_{0.2}O_3$ and $LaNiO_3$, respectively, close to the other high efficient perovskite materials (e. g. 73% of $Sr_{0.95}Ce_{0.05}CoO_{3-\delta}$) and non-precious metal catalysts (e. g. 79% of Fe/N/C).[34, 35] The overpotential of $LaNi_{0.8}Fe_{0.2}O_3$ is lower than that of $LaNiO_3$ by 0.215 V and 0.312 V measured at the middle of discharge/charge of the 1st and 10th cycles, respectively, indicating an obviously improved catalytic activity and cell durability after Fe doping in $LaNiO_3$. The improvement is especially obvious in the OER process, consistent with the half-cell measurements in Fig. 7 (b).

Conclusions

Iron doping in $LaNi_{1-x}Fe_xO_3$ (x = 0, 0.1, 0.2) synthesized by a sol-gel method increases the valence state of the surface Ni and, thereby, the catalytic activity for both the ORR and OER in 0.1 M KOH electrolyte. The Fe-doped $LaNiO_3$ offers a low-cost electrocatalyst for an air cathode in metal/air batteries.

Acknowledgments

John B. Goodenough thanks the Robert Welch Foundation Grant number F-1066. Dawei Zhang thanks the National Natural Science Foundation of China (Grant No. 51472070), Natural Science Foundation of Anhui Province (Grant No. 2012AKZR0355), Scientific Research Foundation for Returned Scholars from Ministry of Education of China (Grant No.2011JYLH1512), and CAS Key Laboratory of Materials for Energy Conversion (Grant No. KF2014004)

Notes and references

[a] School of Chemical Engineering, Hefei University of Technology, Hefei, 230009, P.R. China.
[b] Texas Materials Institute, The University of Texas at Austin, 1 University Station, C2201, Austin, Texas78712.
[c] CAS Key Laboratory of Materials for Energy Conversion, Hefei, 230026, P.R. China.
* Texas Materials Institute, Materials Science & Engineering Program, The University of Texas at Austin.

1 G. Girishkumar, B. McCloskey, A.C. Luntz, S. Swanson, W. Wilcke, *J. Phys. Chem.*, 2010, **14**, 2193-2203.
2 Z. Chen, A. Yu, D. Higgins, H. Li, H. Wang, Z. Chen, *Nano Lett.*, 2012, **12**, 1946-1952.
3 J.-S. Lee, S. Tai Kim, R. Cao, N.-S. Choi, M. Liu, K.T. Lee, J. Cho, *Adv. Energy Mater.*, 2011, **1**, 34-50.
4 J. Christensen, P. Albertus, R.S. Sanchez-Carrera, T. Lohmann, B. Kozinsky, R. Liedtke, J. Ahmed, A. Kojic, *J. Electrochem. Soc.*, 2012, **159**, R1-30.
5 G. Girishkumar, B. McCloskey, A.C. Luntz, S. Swanson, W. Wilcke, *J. Phys. Chem. Lett.*, 2010, **1**, 2193-2203.
6 E. Yoo, J. Nakamura, H. Zhou, *Energy Environ. Sci.*, 2012, **5**, 6928-6932.
7 D. Zhang, Z. Fu, Z. Wei, T. Huang, A. Yu, *J. Electrochem. Soc.*, 2010, **157**, A362-365.
8 L. Zhang, R. Iyyamperumal, D.F. Yancey, R.M. Crooks, G. Henkelman, *ACS Nano*, 2013, **7**, 9168-9172.
9 M. Oezaslan, F. Hasché, P. Strasser, *J. Phys. Chem. Lett.*, 2013, **4**, 3273-3291.
10 Y. Yang, Q. Sun, Y.-S. Li, H. Li, Z.-W. Fu, *J. Power Sources*, 2012, **223**, 312-318.
11 S. Ida, A.K. Thapa, Y. Hidaka, Y. Okamoto, M. Matsuka, H. Hagiwara, T. Ishihara, *J. Power Sources*, 2012, **203**, 159-164.
12 Y.-C. Lu, Z. Xu, H.A. Gasteiger, S. Chen, K. Hamad-Schifferli, Y. Shao-Horn, *J. Am. Chem. Soc.*, 2010, **132**, 12170–12171.
13 R. Chiba, F. Yoshimura, Y. Sakurai. *Solid State Ionics*, 1999, **124**, 281-288.
14 J. Suntivich, K.J. May, H.A. Gasteiger, J.B. Goodenough, Y. Shao-Horn, *Sci.*, 2011, **334**, 1383-1385.
15 J. Suntivich, H.A. Gasteiger, N. Yabuuchi, H. Nakanishi, J.B. Goodenough, Y. Shao-Horn, *Nat. Chem.*, 2011, **3**, 546-550.
16 W. Zhou and J. Sunarso. *J. Phys. Chem. Lett.*, 2013, **4**, 2982-2988.
17 Jaka Sunarso, Angel A. J. Torriero et al. *J. Phys. Chem. C*, 2012, **116**, 5827−5834.
18 A. Costa, M.E.M. Jorge, M.D. Carvalho, A. Gomes, M.I.D. Pereira, *J. Solid State Electrochem.*, 2013, **17**, 2311-2318.
19 Z.-Z. Du, P. Yang, L. Wang, Y.-H. Lu, J.B. Goodenough, J. Zhang, D.W. Zhang, *J. Power Sources*, 2014, **265**, 91-96.
20 C. Jin, X.C. Cao, L.Y. Zhang, C. Zhang, R.Z. Yang, *J. Power Sources*, 2013, **241**, 225-230.
21 S. Zhuang, C. Huang, K. Huang, X. Hu, F. Tu, H. Huang, *Electrochem. Commun.*, 2011, **13**, 321-324.
22 Y. Zhao, L. Xu, L. Mai, C. Han, Q. An, X. Xu, X. Liu, Q. Zhang, *Proc. Natl. Acad. Sci. U. S. A.*, 2012, **109**, 16596-16602.
23 J.B. Goodenough, *Prog. Solid State Chem.*, 1971, 5, 145-399.
24 Chunwen Sun, Rob Hui, Justin Roller, *J Solid State Electrochem.*, 2010, **14**, 1125–1144.
25 J. J. Martin, V. Neburchilov, H. Wang, W. Qu, *Int. J. Elec. Power*, 2009, **1**, 4244-4509.
26 Z. Du, P. Yang, L. Wang, Y. Lu, J.B. Goodenough, J. Zhang, D. Zhang, *J. Power Sources*, 2014, **265**, 91-96.

27 L. Wang, X. Zhao, Y. Lu, M. Xu, D. Zhang, R.S. Ruoff, K.J. Stevenson, J.B. Goodenough, *J. Electrochem. Soc.,* 2011, **158**, A1379-A1382.

28 Y. Lu, J.B. Goodenough, Y. Kim, *J. Am. Chem. Soc.,* 2011, **133**, 5756-5759.

29 K.-N. Jung, J.-H. Jung, W.B. Im, S. Yoon, K.-H. Shin, J.-W. Lee, *ACS Appl. Mater. Interfaces*, 2013, **5**, 9902-9907.

30 W.G. Hardin, D.A. Slanac, X. Wang, S. Dai, K.P. Johnston, K.J. Stevenson, *J. Phys. Chem. Lett.* 2013, **4**, 1254-1259.

31 S.S. Maluf, E.Y. Tanabe, P.A.P. Nascente, E.M. Assaf, *Top. Catal.,* 2011, **54**, 210-218.

32 J. Rossmeisl, Z.W. Qu, H. Zhu, G.J. Kroes, J.K. Nørskov, *J. Electroanal. Chem.,* 2007, **607**, 83-89.

33 D.H. Kim, N.M. Aimon, L. Bi, G.F. Dionne, C.A. Ross, *J. Appl. Phys.* 2012, **111**,07A918.

34 W. Yang, J. Salim, S. A. Li, C. W. Sun, L. Q. Chen, J. B. Goodenough, Y. Kim, *J. Mater. Chem.* 2012, **22**, 18902-18907.

35 J. L. Shui, N. K. Karan, M. Balasubramanian, S. Y. Li, D. J. Liu, *J. Am. Chem. Soc.* 2012, **134**, 16654-16661.

Graphical Abstract

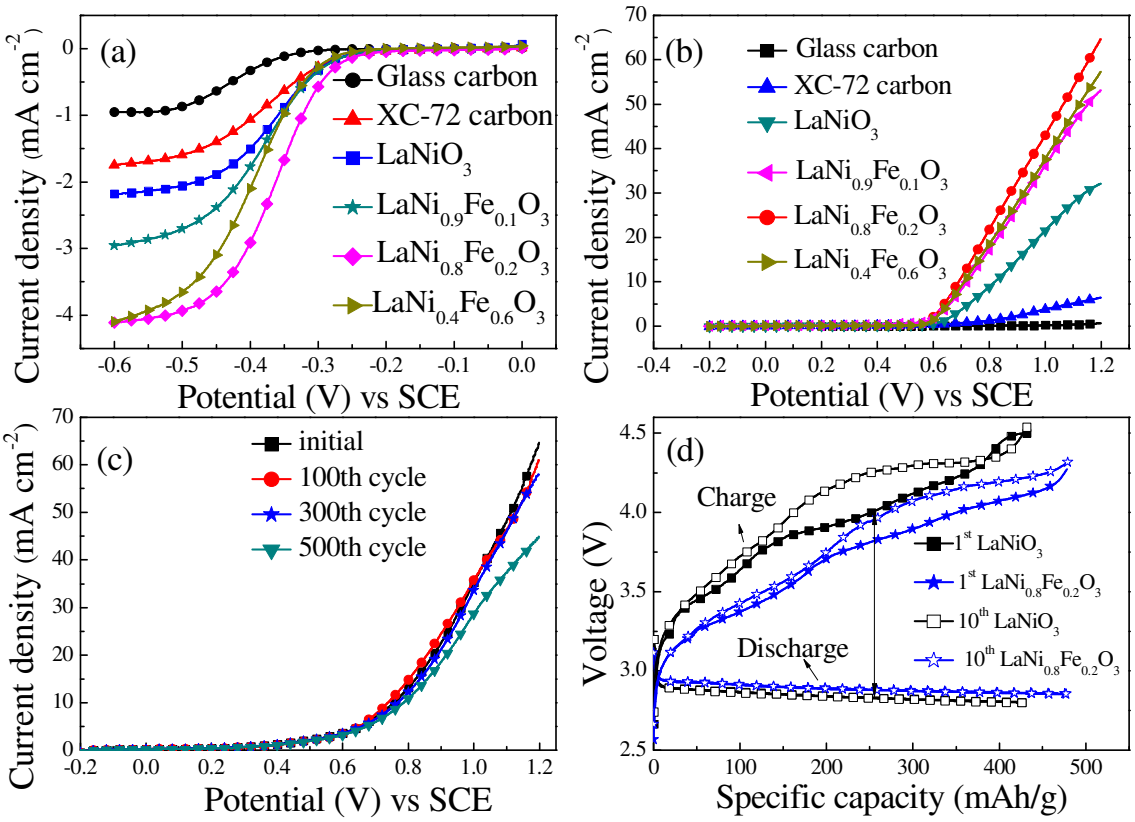

Iron doping in $LaNi_{1-x}Fe_xO_3$ (x = 0, 0.1, 0.2) synthesized by a sol-gel method increases the valence state of the surface Ni and, thereby, the catalytic activity for both the ORR and OER in 0.1 M KOH electrolyte. The Fe-doped $LaNiO_3$ offers a low-cost electrocatalyst for an air cathode in metal/air batteries.